BJ www.biochemj.org

BJ Structure

Biochem. J. (2009) **423**, 209–217 (Printed in Great Britain) doi:10.1042/BJ20090565

Mapping of the ligand-binding site on the b′ domain of human PDI: interaction with peptide ligands and the x-linker region

Lee J. BYRNE*[1], Ateesh SIDHU†[1], A. Katrine WALLIS†, Lloyd W. RUDDOCK‡, Robert B. FREEDMAN†, Mark J. HOWARD*[2] and Richard A. WILLIAMSON*[2]

*Department of Biosciences, University of Kent, Canterbury CT2 7NJ, U.K., †Department of Biological Sciences, Warwick University, Coventry CV4 7AL, U.K., and ‡Department of Biochemistry, University of Oulu, 90570 Oulu, Finland

PDI (protein disulfide-isomerase) catalyses the formation of native disulfide bonds of secretory proteins in the endoplasmic reticulum. PDI consists of four thioredoxin-like domains, of which two contain redox-active catalytic sites (**a** and **a′**), and two do not (**b** and **b′**). The **b′** domain is primarily responsible for substrate binding, although the nature and specificity of the substrate-binding site is still poorly understood. In the present study, we show that the **b′** domain of human PDI is in conformational exchange, but that its structure is stabilized by the addition of peptide ligands or by binding the **x**-linker region. The location of the ligand-binding site in **b′** was mapped by NMR chemical shift perturbation and found to consist primarily of residues from the core β-sheet and α-helices 1 and 3. This site is where the **x**-linker region binds in the X-ray structure of **b′x** and we show that peptide ligands can compete with **x** binding at this site. The finding that **x** binds in the principal ligand-binding site of **b′** further supports the hypothesis that **x** functions to gate access to this site and so modulates PDI activity.

Key words: **b′** domain, ligand-binding site, nuclear magnetic resonance (NMR), protein disulfide-isomerase (PDI).

INTRODUCTION

PDI (protein disulfide-isomerase) is a key enzyme responsible for the formation of native disulfide bonds in proteins that enter the secretory pathway of eukaryotic cells. PDI is a multifunctional protein able to catalyse the oxidation and isomerization of disulfide bonds, as well as to bind to unfolded proteins and act as a molecular chaperone [1]. The isomerization of incorrectly paired cysteine residues is often a rate-limiting step on the folding pathway of disulfide bond-containing proteins both *in vitro* and *in vivo* [2–4]. The ability of PDI to combine redox and molecular chaperone-like activities allows it to bind to partly structured folding intermediates and to catalyse simultaneously protein folding and associated native disulfide bond formation [5]. PDI is the archetype of a large family of ER (endoplasmic reticulum)-resident PDI-like proteins [6].

PDI contains four thioredoxin-like domains, two of which, like thioredoxin itself, have redox-active catalytic sites (**a** and **a′**) and two of which do not (**b** and **b′**). The domain order is **a**-**b**-**b′**-**x**-**a′**-**c**, where **x** is a 19-residue linker between the **b′** and **a′** domains [7] and **c** is a C-terminal acidic tail containing the KDEL (Lys-Asp-Glu-Leu) ER-retention signal. The **a** and **a′** domains are responsible for the redox activity of PDI, whereas the **b′** domain has been shown to be essential for ligand binding [8]. The **b′** domain binds both small and large peptide ligands, although large ligands also require the **a** and **a′** domains to contribute to the overall binding interaction [8,9]. The **b′** domain is likely to control the substrate specificity of PDI and is known to be required for disulfide isomerization reactions in protein substrates [10]. In ERp57, a PDI family member that is specific for the lectin-like molecular chaperones calnexin and calreticulin, the **b′** domain contains the binding site for these proteins allowing the lectins to recruit nascent glycosylated polypeptides to the isomerase to facilitate folding [11,12].

PDI has proved to be a difficult protein for three-dimensional structure determination. The first structure for a full-length PDI (yeast Pdi1p) was not published until 2006 [13], although abundant protein from a variety of sources has been available for many years. This structure was obtained from crystals of yeast Pdi1p grown at 4 °C and revealed a twisted U-shaped molecule where the **b** and **b′** domains make up the valley floor and the **a** and **a′** domain are positioned either side with their redox-active catalytic sites facing one another across the central cleft. The U is lined with hydrophobic residues thought to constitute the ligand-binding site. The **b′** domain provides the core of this putative binding site, with the **a** and **a′** domains contributing hydrophobic residues around their active sites. The **b** domain extends the hydrophobic site on **b′** and may be important for binding larger molecules. A second crystal form of yeast Ppi1p grown at a higher temperature has shown that the full-length molecule is conformationally flexible with respect to the orientation and position of the **a** domain to the rest of the molecule [14]; such flexibility will tend to prevent regular crystal formation.

Single domain structures for domains **a** and **b** of human PDI were determined by NMR more than 10 years ago [15,16], and a structure of the isolated **a′** domain has been deposited in the Protein Data Bank (PDB code 1X5C), but there has been no reported NMR structure for the independent **b′** domain of human PDI. However, recently, six three-dimensional structures of mammalian PDI family members containing a **b′** domain have been published (full-length ERp44 [17], full-length ERp57 in a complex with tapasin [18], **bb′** domains of ERp57 and ERp72

Abbreviations used: ER, endoplasmic reticulum; HSQC, heteronuclear single-quantum coherence; IPTG, isopropyl β-D-thiogalactoside; NBD, nucleotide-binding domain; PDI, protein disulfide-isomerase; Pdi1p, yeast PDI (product of the *Saccharomyces cerevisiae PDI1* gene); SBD, substrate-binding domain; TROSY, transverse relaxation optimized spectroscopy.

[1]These authors contributed equally to this work

[2]Correspondence may be addressed to either of these authors (email m.j.howard@kent.ac.uk or r.a.williamson@kent.ac.uk).

[12,19], and **b′x** and **bb′** domains of human PDI [20,21]). In two of these structures, a hydrophobic site similar to that seen in the **b′** domain of yeast has been identified into which another part of the polypeptide chain is bound (the **x**-linker region in **b′x** [20] and the C-terminal region in ERp44 [17]). These findings suggest that access to the core ligand-binding site can be gated by a capping structure within the protein, leading to the possibility of high- and low-ligand-affinity states.

To date there are no published structures of PDI with bound peptide ligands or unfolded protein substrates and hence the ligand-binding site has not been identified directly. In the present study, we have used NMR chemical shift perturbation to map the ligand-binding site in the **b′** domain of human PDI and have shown that peptide ligands can compete with the **x**-linker region for binding at this site. We also show that the neighbouring **b** domain and **x**-linker region stabilize the structure of **b′** and that the **b** domain has an effect on the ligand-binding site, even though this site is distant from the **b–b′** domain–domain interface.

MATERIALS AND METHODS

Recombinant protein expression and purification

Human PDI fragments comprising **b′** (Pro^{218}–Gly^{332}), **b′x** (Lys^{213}–Pro^{351}), **bb′** (Ala^{119}–Gly^{332}) and **bb′x** (Ala^{119}–Pro^{351}) were expressed from pET23b (Novagen) in *Escherichia coli* BL21(DE3)-pLysS cells with an N-terminal His_6 tag (MHHHHHHM). *E. coli* cultures were grown at 37 °C in M9 minimal medium containing either [^{15}N]ammonium sulfate or [^{15}N]ammonium sulfate and [^{13}C]glucose and induced with 1.0 mM IPTG (isopropyl β-D-thiogalactoside) for 4 h to generate uniformly ^{15}N-labelled and ^{15}N/^{13}C-labelled protein.

For protein purification, cells were harvested by centrifugation at 6200 ***g*** for 15 min and resuspended in 20 mM sodium phosphate buffer (pH 7.3) (buffer A), containing DNase (10 μg/ml) before freezing at −20 °C. Thawed cell lysate was clarified by centrifugation at 17400 ***g*** for 15 min and loaded on to a column of nickel-chelating Sepharose (GE Healthcare). The column was washed with buffer A containing 25 mM imidazole and 0.5 M NaCl following by buffer A alone, and then the recombinant product eluted with buffer A containing 50 mM EDTA. The eluted protein was dialysed against buffer A or diluted 5× with buffer A before loading on to a Source 30Q ion-exchange column (GE Healthcare). Bound proteins were separated with a linear gradient of 0–500 mM NaCl over 20 column volumes. Fractions were pooled based on SDS/PAGE analysis and concentrated by ultrafiltration (5 kDa cut-off for single domain constructs, 10 kDa cut-off for larger constructs).

b′x and **bb′x** constructs were purified further by gel-filtration chromatography. Samples were separated on Superdex 75 or 200 columns (2.6 cm × 55 cm, GE Healthcare) in 20 mM sodium phosphate buffer (pH 7.1) containing 150 mM NaCl. Fractions corresponding to monomer and dimer were well-resolved and were pooled separately.

To prepare triple-labelled (^{2}H, ^{13}C, ^{15}N) **bb′x**, a single colony of cells carrying the **bb′x** expression plasmid was grown overnight in 20 ml of M9 minimal medium; cells were then pelleted and resuspended in 40 ml of M9 minimal medium containing 35 % ^2H_2O. Cells from this culture were collected and stored in 40 % glycerol, and the process of adaptation was repeated stepwise using successive cultures in 65, 86, 91, 94 and 96 % ^2H_2O. Cells adapted to growth in 96 % ^2H_2O were streaked on an LB (Luria–Bertani) agar plate with appropriate antibiotics to enable selection of a single colony to inoculate a 50 ml starter culture of M9 minimal medium containing 96 % ^2H_2O, [^{15}N]ammonium sulfate and [^{13}C]glucose supplemented with 10 % Spectra 9 (Spectra Stable Isotopes), a rich medium containing ^{2}H (> 97 %), ^{13}C (> 98 %) and ^{15}N (> 98 %). After overnight growth, this starter culture was used to inoculate two 400 ml cultures of the same medium and these cultures grown to a D_{600} of 0.6 before induction with 1.0 mM IPTG for 6 h. The labelled **bb′x** protein was recovered and purified as described above. The mass of the purified product was determined to be 30180 Da, implying 63 % labelling with ^{2}H (81 % labelling of non-exchangeable ^{1}H) if the labelling efficiency with ^{13}C and ^{15}N was 96 % as determined in previous experiments in water.

NMR spectroscopy

NMR samples were typically 0.5–1.5 mM protein in 20 mM sodium phosphate buffer containing 100 or 150 mM NaCl (pH 6.5) and 10 % (v/v) ^2H_2O in a final volume of 330 μl. Unless stated otherwise, NMR experiments were performed at 600 MHz using a Varian Unity INOVA equipped with a 5 mm HCN z-pulse field gradient probe. All NMR experiments were solvent-suppressed to reduce the water signal using the WATERGATE method [22], and all indirect NMR dimensions [non-TROSY (transverse relaxation optimized spectroscopy) experiments] were acquired using the hypercomplex method. ^{15}N/^{1}H-HSQC (heteronuclear single-quantum coherence) spectra were collected at 25 and 40 °C as described by Alanen et al. [23]. Backbone chemical shift assignment for **b′x** (at 25 °C) and **bb′x** (at 40 °C) were carried out using three-dimensional CBCANH and CBCA(CO)NH experiments [24,25]. Assignments for **bb′x** were also confirmed by analysis of three-dimensional TROSY-HNCA and TROSY-HN(CO)CA experiments acquired at 800 MHz (Varian Unity INOVA) and 25 °C on a deuterated sample prepared as described above. Backbone assignments for **b** were taken from the BioMagResBank (accession code 4156 [26]) and the assignments confirmed and mapped on to an ^{15}N/^{1}H-HSQC spectrum of **b** collected under the same experimental conditions as the other constructs by analysis of ^{15}N HSQC-TOCSY and ^{15}N-HSQC-NOESY spectra. All NMR data were processed using NMRPipe [27], and spectra were analysed manually using the CCPN Analysis software package [28].

Peptide ligands

Δ-Somatostatin (AGSKNFFWKTFTSS [8]) and KFWWFS were generated by peptide synthesis and purified by reverse-phase HPLC. Peptide was added at a 2-fold molar excess over target protein concentration unless stated otherwise.

RESULTS

Expression and purification of b′, b′x, bb′ and bb′x

PDI domain fragments were purified by a combination of nickel-affinity and anion-exchange chromatography. **b′x** and **bb′x** often gave complex or asymmetric peak profiles during ion-exchange chromatography (Figure 1a), suggesting the presence of two or more forms, although SDS/PAGE and electrospray ionization–MS analysis on fractions taken across the peak revealed only a single protein species at the correct molecular mass (Figure 1a, inset). Subsequent analysis of ion-exchange-purified material by gel-filtration chromatography found that preparations of **b′** and **bb′** resolved as a single peak (results not shown). In contrast, **b′x** and **bb′x** both resolved as two peaks of approximately equal magnitude (Figure 1b). These subfractions represent dimeric and monomeric forms of **b′x** and **bb′x**, whereas **b′** and **bb′**

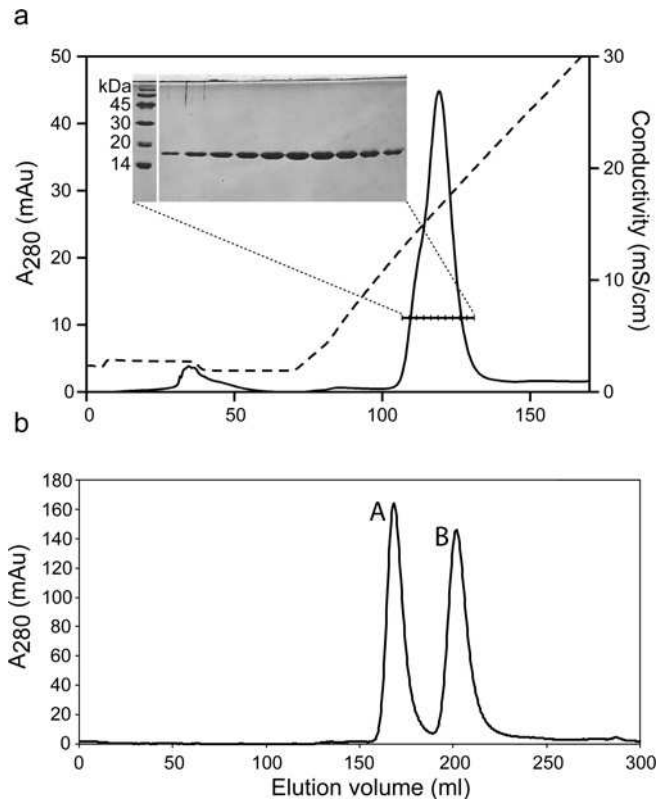

Figure 1 Purification of b′x

(**a**) Typical asymmetric ion-exchange profile of **b′x** with SDS/PAGE analysis of fractions taken across the peak shown in the inset (molecular masses are indicated in kDa). The broken line (right-hand axis) indicates the salt gradient used for elution (0 – 0.5 M NaCl). (**b**) Gel-filtration chromatography of the **b′x** peak shown in (**a**). **b′x** resolves into two peaks identified as homodimer (A) and monomer (B). mAu, milli-absorbance units.

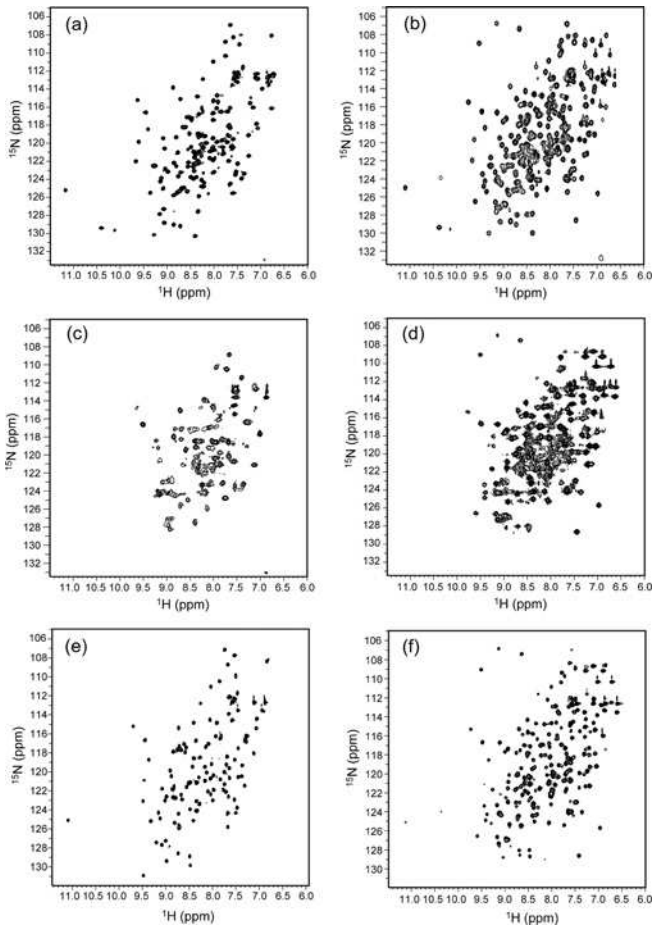

Figure 2 ^{15}N/^{1}H-HSQC spectra of (a) b′x, (b) bb′x (c) b′, (d) bb′, (e) b′ + KFWWFS and (f) bb′ + Δ-somatostatin

All spectra were collected at pH 6.5 and 25 °C. **b′** and **bb′** were found to be exclusively dimeric on purification, whereas **b′x** and **bb′x** were found to be both dimeric and monomeric (only spectra for the monomeric form shown here). Some 20 non-overlapping peaks common to **b′**/**b′x** or **bb′**/**bb′x** spectra were used to estimate average F_2 line width at half peak height. The estimates obtained were: **b′x** = 20.1 Hz, **bb′x** = 24.0 Hz, **b′** > 40 Hz, **bb′** = 36.9 Hz, **b′** + KFWWFS=18.5 Hz and **bb′** + Δ-somatostatin=26.4 Hz.

are found exclusively as dimeric species. Both **b′x** and **bb′x** contain a unique tryptophan residue in the **x**-linker region of the fragment, and fluorescence analysis of the monomeric and dimeric forms revealed spectra similar to those seen previously for the 'capped' and 'uncapped' forms of **b′x** respectively [20]. We have previously determined the structure of the capped form of **b′x** using X-ray crystallography. This structure shows the **x**-linker bound in a hydrophobic patch on the surface of **b′** [20]. The monomeric fractions of **b′x** and **bb′x** gave well-resolved NMR spectra, consistent with folded proteins (Figures 2a and 2b). All the work in the present study was carried out using purified samples of monomeric **b′x** and **bb′x** and dimeric **b′** and **bb′**.

Backbone assignment of b′x and bb′x

Backbone assignments were obtained from standard triple-resonance datasets acquired at 25 °C for **b′x** and 40 °C for **bb′x** (the elevated temperature for **bb′x** was to compensate for signal reduction from increased NMR relaxation rates owing to the higher molecular mass of this construct). Backbone assignments for **bb′x** were confirmed by analysis of TROSY-HNCA and TROSY-HN(CO)CA experiments using an 81 % non-exchangeable deuterated sample. A series of ^{15}N/^{1}H-HSQC experiments for **bb′x** at 40, 35, 30 and 25 °C enabled extrapolation of assignments for comparison with **b′x** chemical shift data at 25 °C. Assignments for both constructs have been deposited in the BioMagResBank (accession codes 15998 and 15974 for **b′x** and **bb′x** respectively).

Backbone assignment for the **x**-linker region in both constructs proved to be more challenging than for the rest of the molecule with resonances weak or lacking from the CBCANH and/or CBCA(CO)NH experiments. In **b′x**, two assignment pathways were observed for residues Met^{339}–Gln^{350}, suggesting at least two structural forms for this region. One pathway consisted of sharp well-resolved peaks; the second pathway consisted of broader peaks more typical in line width to those of the rest of the protein. These two sets of peaks are believed to originate respectively from a (freely mobile) unbound **x**-linker region and a bound form of **x** which interacts with a site on the **b′** domain. In contrast, the **bb′x** spectra revealed only one detectable assignment pathway for the **x**-linker region, although a few unassignable peaks remain in the spectra. The line widths for the peaks in the assigned pathway were narrower compared with the rest of the protein, suggesting that they originate from an unbound form of **x**. Furthermore, the last five residues (Asp^{346}–Gln^{350}) had comparable backbone chemical shifts with unbound **x** in **b′x**. The signals from an unbound **x**-linker region are thought to arise from small amounts of uncapped dimer contaminating the samples. Uncapped **x** gives a characteristic high-field indole amide peak which can be seen in

the $^{15}N/^{1}H$-HSQC spectra ($^{1}H_N = 10.13$ p.p.m., $^{15}N = 129.8$ p.p.m.; Figure 2b). The sharp resonances of the uncapped **x**-linker region allow it to be detected easily, even when in relatively low amounts.

Effect of peptide ligands on the structure of b′ and bb′

The NMR spectra for dimeric **b′** and **bb′** were poor and their broad line widths prevented backbone assignment (Figures 2c and 2d). However, in the presence of a peptide ligand (Figures 2e and 2f), the line shape, resolution and dispersion of these spectra improved markedly, suggesting dissociation of the dimeric form to generate monomers, together with possible ligand-dependent stabilization of the **b′** structure reducing any line-broadening from conformational exchange. The hydrophobic peptide KFWWFS was found to have a significant effect on **b′** (compare Figures 2c and 2e), giving spectra with line widths comparable with capped **b′x** (Figure 2a; average line widths given in the legend to Figure 2), but this ligand proved to be very difficult to handle reliably owing to its poor solubility. An alternative ligand, Δ-Somatostatin [8], was used for studies with **bb′**, and this ligand also had a significant effect on the line widths (compare Figures 2d and 2f), giving values approaching those seen for capped **bb′x** (Figure 2b). Δ-Somatostatin was also seen to improve the quality of spectra when added to **b′**, but the effect was less marked than when added to **bb′** at the same concentration and significantly poorer than that seen with KFWWFS (results not shown). Experiments were also carried out with the small hydrophobic molecule 2-propylphenol that had been shown previously to interact with the **b′** domain of PDI [29]. This molecule was seen to improve the spectrum of **b′** (results not shown), with average line widths decreasing to 24.4 Hz.

Mapping of the b′ ligand-binding site

Chemical shift perturbation can be estimated, when comparing spectra where only one of the spectra has been fully assigned, by measuring distances from signals in the assigned spectrum to the nearest peak in the unassigned spectrum. This approach was used to identify the ligand-binding site in **b′** by comparing the assigned $^{15}N/^{1}H$-HSQC spectrum of **b′x** with **b′** + KFWWFS and the assigned spectrum of **bb′x** with **bb′** + Δ-somatostatin. The direct comparison of **b′** with **b′** + KFWWFS or **bb′** with **bb′** + Δ-somatostatin was not possible because of the poor quality of the unliganded spectra (Figures 2c and 2d). The Δ-somatostatin ligand was also seen to bind to **b′x** as judged by peak shifts in $^{15}N/^{1}H$-HSQC spectra, hence a similar nearest-peak analysis was carried out for **b′x** with **b′x** + Δ-somatostatin.

The minimal chemical shift changes seen for the backbone amide resonances of **bb′** generated by comparing spectra for **bb′x** with **bb′** + Δ-somatostatin are shown in Figure 3(a). The data show that the majority of the chemical shift perturbation maps to the **b′** domain, a finding consistent with the **b′** domain containing the ligand-binding site [7,8]. In general, the background level of chemical shift change is much higher in **b′** than in **b**, suggesting some global movement or behaviour change within the structure; however, the most substantial changes are seen in the regions Glu^{222}–Ile^{240}, Leu^{270}–Phe^{271}, Leu^{300}–Thr^{302}, Tyr^{310}–Lys^{311} and a number of residues at the C-terminus (e.g. Cys^{326} and Arg^{328}). A very similar pattern of shifts is seen for the comparisons between **b′x** and **b′** + KFWWFS (Figure 3b), and **b′x** and **b′x** + Δ-somatostatin (Figure 3c), although the magnitude of the shifts for the most perturbed residues in both analyses appears to be somewhat diminished. The comparison of **b′x** with **b′x** + Δ-somatostatin is the only comparison where the analysis includes the **x**-linker region (this region was omitted from the other two analyses as it is absent in the liganded construct). Chemical shift

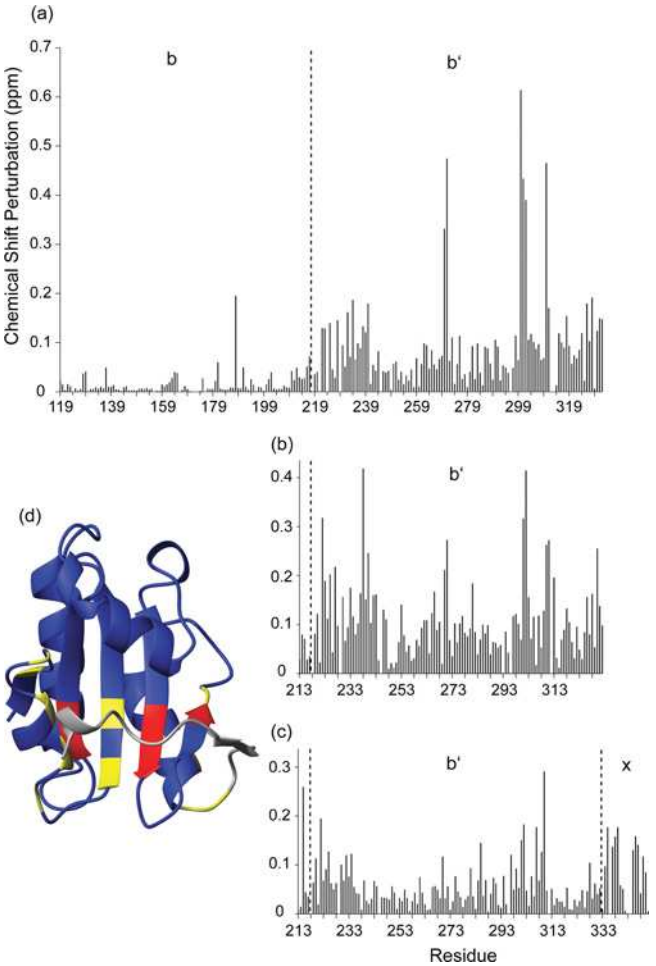

Figure 3 Chemical shift perturbation (to nearest peak) for backbone amide $^{1}H_N$ and ^{15}N resonances of (a) bb′x compared with bb′ + Δ-somatostatin, and mapped on to the crystal structure of b′x (d), (b) b′x compared with b′ + KFWWKS and (c) b′x compared with b′x + Δ-somatostatin

Where the **x**-linker region was not part of the liganded construct [comparisons (**a**) and (**b**)], this region was removed from the nearest-peak analysis. Chemical shifts for the bound form of **x** were used for comparison (**c**). The magnitude of the chemical shift change was determined as $|\Delta^{1}H_N| + |\Delta^{15}N/6|$ and the domain boundaries are shown by the vertical broken lines. (**d**) Perturbed residues from **bb′x** compared with **bb′** + Δ-somatostatin (**a**) mapped on to the crystal structure of **b′x** [20] (yellow, > 0.13 p.p.m.; red, > 0.2 p.p.m.). The **x**-linker region is shown in grey. Figure produced using MOLMOL [35].

perturbations are seen in the **x**-linker region on the addition of Δ-somatostatin to **b′x** (Figure 3c), which is consistent with **x** being displaced by the peptide ligand. Peaks with significant shifts in the **x**-linker region are Ile^{334}–Asp^{348}. This stretch of residues comprises the majority of the **x**-linker region and includes a β-strand that forms an antiparallel connection with β5 in the core β-sheet. Corresponding chemical shift changes are seen in β5 (Met^{307}–Tyr^{310}) when **x** is displaced from the ligand-binding site by Δ-somatostatin.

The shifted residues in Figure 3(a) are shown mapped on a ribbon diagram of the crystal structure of **b′x** in Figure 3(d). Those residues showing the greatest backbone amide shifts are shown in red, whereas those with moderate shifts are shown in yellow. The analysis reveals that the majority of the shifted residues are in the vicinity of where **x** contacts the **b′** domain; Thr^{238}, Ile^{240}, Leu^{270}, Phe^{271}, Leu^{300}–Thr^{302} and Tyr^{310} are in the β-sheet that forms the floor of the binding site, and Ala^{228} and Phe^{232} form the

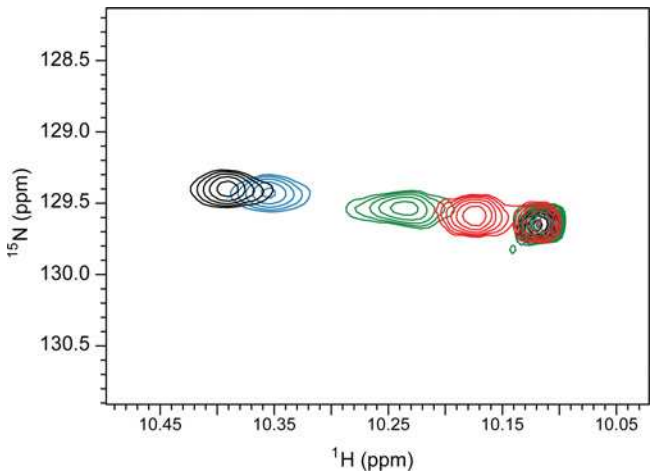

Figure 4 Perturbation of the indole resonances of Trp^{347} from b′x in the presence of increasing concentrations of Δ-somatostatin

Black, no Δ-somatostatin; blue, 0.18 mM Δ-somatostatin (0.7:1 molar ratio to **b′x**); green, 0.76 mM Δ-somatostatin (1.9:1 molar ratio to **b′x**); red, 0.9 mM Δ-somatostatin (3.0:1 molar ratio to **b′x**). The high-field peak ($^{1}H_N = 10.12$ p.p.m.) is generated by the uncapped form of **b′x** where the **x**-linker region is believed to be unbound, whereas the low-field resonance ($^{1}H_N = 10.39$ p.p.m. in the absence of Δ-somatostatin) is the capped form of the protein where the **x**-linker region is bound in the ligand-binding site. All four spectra show an overlaid signal for the uncapped form (far-right-hand peak) which results from small amounts of **b′x** dimer in the samples.

face of α1 that borders the C-terminal end of the binding site. Moderate shifts are also seen at the base of α4 that continues into the **x**-linker region; chemical shift changes between **bb′x** and **bb′** + Δ-somatostatin in this region may not reflect ligand binding, but may be a direct consequence of **x** truncation in the **bb′** construct.

Effect of ligand binding on x

The **x**-linker region contains a unique tryptophan residue (Trp^{347}) and the indole cross-peak from this tryptophan side chain was used previously to detect the difference in environment of the **x**-linker region between the 'capped' and 'uncapped' forms of the **b′x** domain [20]. Samples of capped **b′x** typically contain a small proportion of uncapped dimeric material and hence two peaks for the tryptophan indole are seen (Figure 2a). The low-field cross-peak ($^{1}H_N = 10.39$ p.p.m.) is representative of the monomeric capped conformer, and the sharper high-field cross-peak ($^{1}H_N = 10.12$ p.p.m.) representative of the uncapped dimeric form. Interconversion between the two forms is very slow as shown by the presence of two distinct indole peaks in the HSQC spectra. The addition of Δ-somatostatin to samples of (predominantly) monomeric **b′x** was seen to shift the capped indole peak towards that of the uncapped form which remained unchanged in position and appearance (Figure 4). Furthermore, the degree of shift was dependent on the amount of Δ-somatostatin added to the sample. These results confirm that Δ-somatostatin is able to displace **x** from the ligand-binding site and that the tryptophan side chain in the capped monomer is in fast exchange between two or more conformational states.

Chemical shifts of b and b′x compared with bb′x

NMR chemical shifts provide a convenient way of identifying structural changes in the individual **b** and **b′x** domains when part of the larger **bb′x** construct. The effect of **b′x** on the conformation of **b** was investigated by comparing **b** peak positions in ^{15}N/^{1}H-HSQC spectra of **b** alone and **bb′x** (Figure 5a); similarly, the effect of **b** on **b′x** was investigated by comparing **b′x** peak positions in spectra of **b′x** alone and **bb′x** (Figure 5b).

b′x had little effect on **b** outside of those residues in the interface region. Residues Leu^{188}–Arg^{196} and Leu^{219}–Ala^{228} sensed an environmental change (Figure 5a), but these regions map to the turn between β4 and β5 which is in close proximity to **b′** in the **bb′** structure (Figure 5c) and to a region which extends beyond the domain boundary at Leu^{217}. The lack of significant chemical shift perturbations in **b** outside of the regions in close contact with **b′** suggests that the **b** domain is not structurally influenced by the presence of **b′**.

In contrast, **b′x**, when together with **b** in the **bb′x** construct, did show regions of backbone perturbation outside the immediate interface site. The N-terminus (Lys^{213}–Val^{220}) includes the short linker between the domains and is therefore part of the interface site, but residues Thr^{279}–Glu^{286} and Lys^{335}–Gln^{350} also experienced an environment change and are more distant from **b** (Figure 5b). Thr^{279}–Glu^{286} maps to α3 which forms part of the hydrophobic binding site in **b′** and Lys^{335}–Glu^{350} maps to the **x**-linker region that interacts at this site (Figure 5d). Their perturbation reports on the binding of **x** and suggests that **x** behaves differently in **b′x** compared with **bb′x**. Only backbone chemical shifts for the unbound form of **x** could be assigned for **bb′x** so the perturbation of **x** may reflect the bound/unbound nature of this region in the two datasets. However, it is unlikely that the assignments for α3 are for the uncapped dimer form as these peaks would be expected to be both broader and significantly weaker than the monomeric capped form, since the uncapped dimer was only present at low levels in the purified sample.

DISCUSSION

The key outcome from the present study is the definition of ligand-binding residues in the **b′** domain of human PDI, and the demonstration that these are precisely the residues that interact with the adjacent **x**-linker region of PDI in the 'capped' form of the **b′x** construct, supporting the conclusion that the **x**-linker region gates ligand access to the principal binding site on **b′** [20]. However, this observation was dependent on generating appropriate PDI preparations that gave well-resolved NMR spectra, and this required detailed characterization of several domain combinations and the resolution of multiple forms. Hence the results also provide insights into the dynamics and dimerization behaviour of PDI fragments containing the **b′** domain.

Oligomerization and conformational flexibility of b′-containing fragments

Previous work has shown that chemically homogeneous wild-type **b′x** preparations contained more than one species, as judged by intrinsic fluorescence [7,20]. We have now shown, for both **b′x** and **bb′x**, that two forms can be separated and characterized, a monomeric form that is predominantly in the 'capped' conformation and a dimeric form that is 'uncapped'. In contrast, recombinant **b′** and **bb′** fragments existed exclusively as dimers when purified from *E. coli* cell lysates.

The line widths observed for the various **b′** domain-containing species analysed here are in the order **b′** dimer > **bb′** dimer ≫ **bb′x** monomer > **b′x** monomer (see the legend to Figure 2), although the molecular sizes are in the order **bb′** dimer ≫ **bb′x** monomer > **b′** dimer ≫ **b′x** monomer. The anomalously broad line

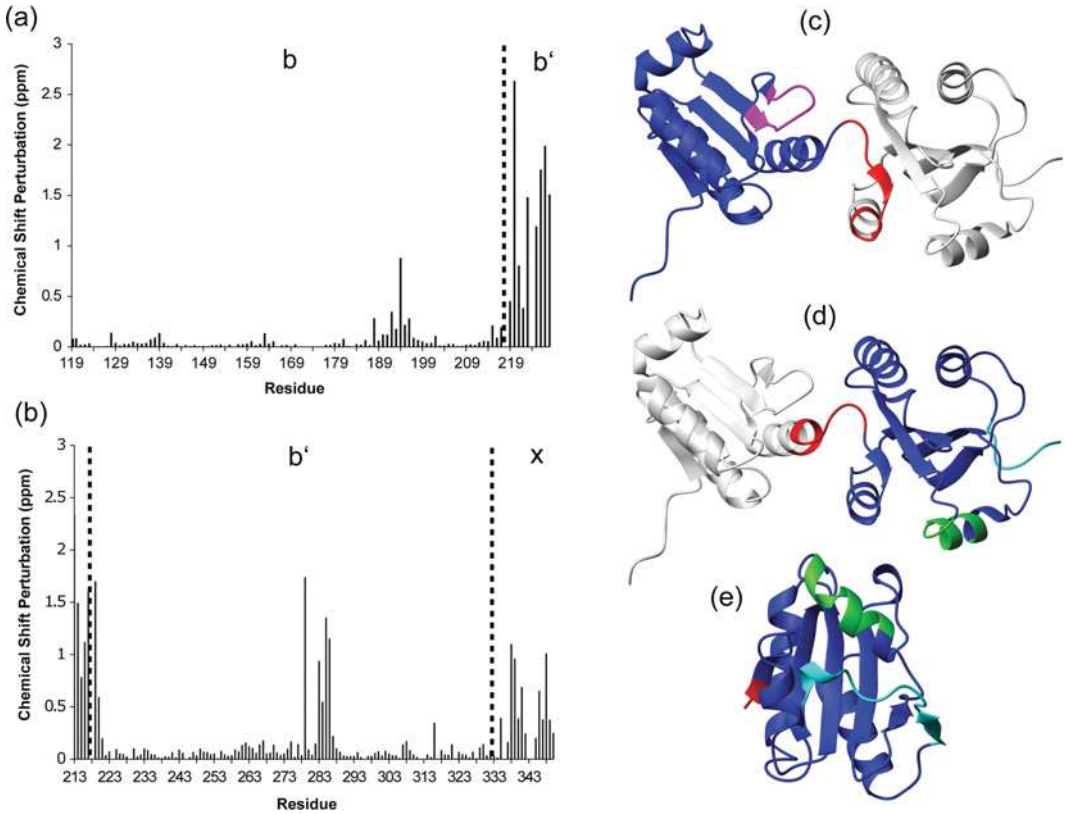

Figure 5 Chemical shift perturbation of backbone amide $^{1}H_{N}$ and ^{15}N resonances of (a) b and (b) b′x in the bb′x di-domain construct compared with the independent domains

The magnitude of the chemical shift change was determined as $|\Delta^{1}H_{N}| + |\Delta^{15}N/6|$. Chemical shifts for the bound form of **x** were used in comparison (**b**) and the domain boundaries are shown by vertical broken lines. (**c** and **d**) The residues perturbed in **b** and **b′x** are shown mapped on to the structure of **bb′** from human PDI [21]. In (**c**), the regions Leu^{188}–Arg^{196} and Leu^{219}–Ala^{228} of **b** are shown in magenta and red respectively, in (**d**) the regions Lys^{213}–Val^{220}, Thr^{279}–Glu^{286} and Lys^{335}–Gln^{350} in **b′x** are shown in red, green and cyan respectively. The part of the di-domain construct not directly involved in the comparison is drawn in light grey. (**e**) The residues perturbed in **b′x** are also shown mapped on to the crystal structure of **b′x** [20] to show their relationship to **x** when bound in the ligand-binding site (residues are coloured according to (**d**) above; **x** is seen in cyan running horizontally across the β-sheet in the centre of the diagram). Figure produced using MOLMOL [35].

widths observed for the **b′** dimer suggest that the **b′** domain is in conformational exchange; line broadening is seen throughout the **b′** spectrum (Figure 2c), suggesting that this dynamic flexibility affects all residues and is not ameliorated by homodimer formation. Interestingly, the **bb′** construct showed narrower line widths than **b′**, even though it is twice the molecular size of **b′** and also forms a homodimer. It therefore appears that the **b** domain is able to stabilize the **b′** conformation and this stabilization may occur partly through intermolecular interactions within the **bb′** dimer. The second crystal structure for yeast Pdi1p represents a dimeric form of the full-length protein [14] and shows intermolecular interactions between **b** and **b′** domains that include hydrophobic residues from the ligand-binding site. Similar interactions within the human **bb′** homodimer could stabilize the structure and so account for the narrower line widths seen for **bb′** compared with **b′**. Conversely, our comparison of NMR chemical shifts between the monomeric species **b′x** and **bb′x** (see above) indicates direct effects of the **b** domain on the adjacent **b′** domain, so intramolecular stabilization effects may also contribute to the differences in line width of **b′** residues between **b′** and **bb′**. It is interesting to note, with regard to the conformational flexibility observed for the **b′** domain, that structural disorder is a common feature of ligand-binding regions of molecular chaperones [30].

The ligand-binding site in the b′ domain

The ligand-binding site of PDI has not been identified directly from structure determination of PDI–ligand complexes, but has been inferred from the ligand-binding activity of domain combinations and mutants [7,8], and by the identification of hydrophobic surface patches [13]. The site mapped in the present study by chemical shift perturbation on ligand binding is in good agreement with the hydrophobic site identified on the surface of the **b′** domain in the yeast Pdi1p structure (Figure 6). The definition of the site mapped by chemical shift perturbation is broader than that of the hydrophobic surface in Pdi1p, but this reflects the nature of the analysis where the perturbation data highlight changes to the environment of the protein backbone as sensed by the $^{1}H_{N}$ and ^{15}N amide nuclei and not directly by the side chains. It is now clear that the site where peptide ligands bind is also the site where the **x**-linker interacts in the **b′x** structure [20]. This finding further supports the idea that the **x**-linker region could act to gate access to the ligand-binding site in human PDI just as the C-terminal region of ERp44 has been shown to cap the ligand-binding site of this PDI family member and compete with exogenous peptide ligands [17].

Δ-Somatostatin was shown to compete with **x** for the ligand-binding site on **b′** (Figure 4). The NMR results suggest that

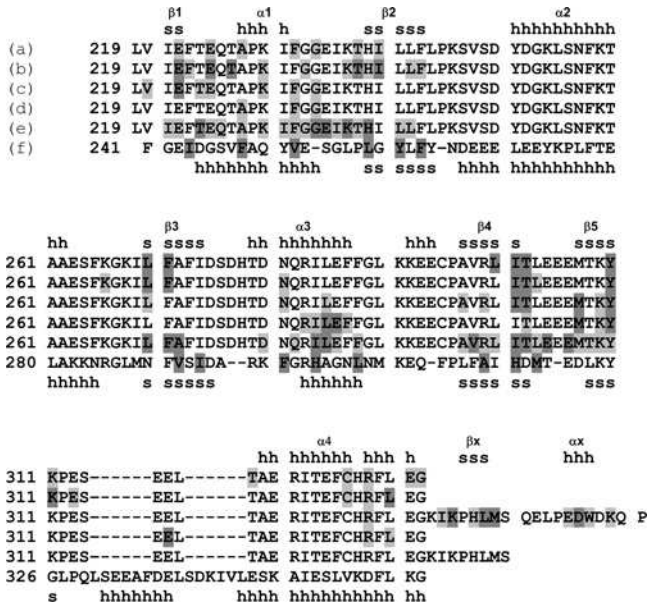

Figure 6 Structural alignment of the b′ domain of human and yeast PDI showing the ligand-binding site as mapped by chemical shift perturbation

(**a**) Comparison of **bb′x** with **bb′** + Δ-somatostatin (light grey, > 0.13 p.p.m.; mid-grey, > 0.2 p.p.m.). (**b**) Comparison of **b′x** with **b′** + KFWWFS (light grey, > 0.15 p.p.m.; mid-grey, > 0.2 p.p.m.). (**c**) Comparison of **b′x** with **b′x** + Δ-somatostatin (light grey, > 0.09 p.p.m.; mid-grey, > 0.15 p.p.m.). (**d**) Comparison of **bb′x** with **bb′** as assigned by Denisov et al. [31] (light grey, > 0.15 p.p.m.; mid-grey, > 0.3 p.p.m.). (**e**) Chemical shift perturbation seen for **bb′** binding to unfolded RNase [21]. (**f**) Hydrophobic ligand-binding site identified in the crystal structure of yeast PDI (mid-grey shading). The secondary-structure assignments for both the human and yeast structures are shown above and below the corresponding sequence. h, α-helix; s, β-sheet.

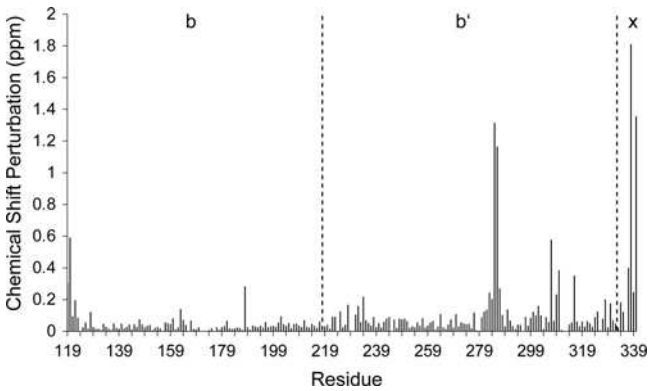

Figure 7 Chemical shift difference map for the backbone amide resonances of bb′x (the present study) and bb′ (as assigned by Denisov et al. [31])

The **bb′** construct contains the first eight residues of the **x**-linker region which is insufficient to extend into the hydrophobic ligand-binding site. The magnitude of the chemical shift change was determined as $|\Delta^1H_N| + |\Delta^{15}N/6|$, and the domain boundaries are shown by vertical broken lines.

the binding of **x** is in fast exchange on the NMR timescale as a chemical shift titration producing an averaged peak position is seen for the tryptophan indole resonance upon addition of ligand. The competing ligand changes the proportion of bound and unbound forms of **x** and so shifts the averaged peak position. The indole peak in different peptide ligand concentrations is seen to shift in a line between the unbound conformation (assumed to have the same ^{15}N and ^1H_N resonances as the uncapped contaminant) and the maximally capped form seen when no competing ligand is present. The proposed fast-exchange properties of the tryptophan indole peak are consistent with our finding that this resonance is virtually devoid of NOEs (nuclear Overhauser effects) to other residues in the protein in a ^{15}N-edited NOESY experiment. Exchange of **x** between two or more forms would broaden any NOESY signals and so make them difficult to detect. From the data presented in Figure 4, the dissociation constant for the **b′x**–Δ-somatostatin complex is in the range 0.1–1.0 mM. This affinity is similar to that of mastoparan (0.13 mM), and slightly weaker than the related peptide somatostatin (0.035 mM), binding to a fragment of PDI containing **b** and **b′** domains ([21]; and further description of the construct below). Sites elsewhere in the full-length protein, such as those identified around the redox-active sites in the **a** and **a′** domains [13], will contribute significantly to the overall binding affinity of PDI to larger unfolded protein substrates.

Comparison with data from an alternative construct

Purification and NMR structural data have recently been published for a construct of human PDI that is intermediate in length between the **bb′** and **bb′x** constructs described in the present study. The protein investigated by Denisov et al. [21] comprises the **bb′** domains and extends for an additional eight residues at the C-terminus compared with the **bb′** fragment in the present study, thus including approximately half of the **x**-linker region [21]. This construct (extended **bb′** or truncated **bb′x**?) was isolated as monomeric and dimeric species that could be separated by gel-filtration chromatography; therefore the first eight residues of **x** are sufficient for the stable formation of the monomeric form. Interestingly, the first eight residues of **x** include a β-strand known to make antiparallel interactions with the core β-sheet of the **b′** domain [20]; however, this strand is not evident in the NMR structure determined for the extended **bb′** construct [21]. It is likely that this strand forms only transiently, or not at all, without the additional stabilizing interactions made by the second half of the **x**-linker region [20].

The monomeric form of the extended **bb′** construct gave NMR spectra of similar resolution to those found by us for **bb′x**, as judged by simple comparison of $^{15}N/^1H$-HSQC data (Figure 2b and [31]). Comparison of the published backbone assignments for the extended **bb′** fragment [31] with our data for **bb′x** showed a close agreement except for the regions known to be involved in the interaction with **x** in the capped conformer (Figure 7). This is to be expected, as the **bb′** fragment does not possess the second half of the **x**-linker region that interacts with the hydrophobic ligand-binding site; hence a comparison is being made between structures where **x** is bound and unbound. The regions that show the greatest difference are Arg^{283}–Phe^{287}, Met^{307}–Tyr^{310} and Glu^{316}. These regions map to α3 which interacts with **x** in the ligand-binding site and the β-strand (Met^{307}–Lys^{311}) which forms an antiparallel interaction with the first half of **x** in **bb′x**, but not in **bb′** (see the previous paragraph).

The backbone assignments for the extended **bb′** construct show two separate pathways from Lys^{333}, the start of the **x**-linker region [31]. This finding is consistent with our findings for **b′x** and **bb′x** and suggests that the shortened **x**-linker region of this construct exists in more than one conformation, as we have observed for **b′x** and **bb′x**.

Denisov et al. [21] have also mapped the ligand-binding site on their extended **bb′** construct of human PDI using chemical shift perturbation and employing Δ-somatostatin, mastoparan and 'scrambled' RNase as ligands. The site defined in their work is very similar to ours (see Figure 6 for a direct comparison). The

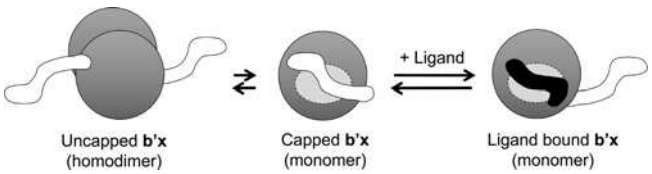

Figure 8 Interactions of the hydrophobic ligand-binding site of the b′ domain of PDI

The example given here is for the **b′x** construct. The peptide ligand (black) is able to displace the **x**-linker region (white) from the hydrophobic binding site (grey). Uncontrolled exposure of the binding site is likely to result in homodimerization; a conformation seen for all the **b′**-containing constructs of the present study. The binding of **x** to the hydrophobic binding site prevents dimer formation and hence the *in vitro* rate of conversion of capped monomer into uncapped dimer was found to be very low. An 'uncapped monomer' state is presumed to exist as a transient intermediate between the monomer states depicted (capped, ligand-bound) and the uncapped dimer, but it is not shown since we have no evidence that it exists in detectable quantities under the conditions we have studied.

most significant difference between the datasets is that Denisov et al. [21] observed chemical shift changes in $\alpha 3$ which runs along the top of the ligand-binding site as shown in Figure 5(d), whereas we saw very few shifts in this region (with the exception of Asn^{281} and Leu^{285}). The lack of perturbation in the present study suggests that there is limited environmental change sensed by the protein backbone in this region when **x** is displaced by a peptide ligand (as in the present study) compared with when a ligand is bound directly by a 'naked' domain where the **x**-linker region is truncated.

Control of access to the binding site on the b′ domain of PDI

Chaperones and folding catalysts face an issue concerning how to control exposure of the hydrophobic sites by which they interact with their substrates. If such a site is fully exposed, then there is a clear risk of uncontrolled binding, and the possibility of dimerization and even aggregation. One strategy to avoid these problems might be for such a site to be capped or otherwise concealed in the absence of substrate. We do not have sufficient structural information on a range of chaperones in the presence and absence of their substrates to test this or to analyse the various structural strategies by which it might be achieved. However, in the case of PDI and ERp44, it does appear that the primary ligand-binding site on the **b′** domain is masked or 'capped' by interaction with an adjacent mobile region. Binding of substrate will then displace the 'cap' providing conditional access to the binding site, which is never fully exposed. A cartoon depicting the displacement of **x** by a peptide ligand from the substrate binding site on **b′x** is shown in Figure 8. This model for PDI and ERp44 is similar to that proposed for the Hsp70 (heat-shock protein 70) family chaperones [32], where a hydrophobic sequence that links the NBD (nucleotide-binding domain) to the SBD (substrate-binding domain) has been observed in two alternative conformations: an 'out' conformation in which the linker is exposed to solvent, and an 'in' conformation in which the linker is packed on to a hydrophobic patch on the SBD. In this case, binding of ATP to the NBD is thought to act allosterically to shift the balance between these two alternative conformations of the interdomain linker and hence control the binding of ligands to the SBD.

At this point, it is difficult to predict whether this strategy of ligand displacement of a local 'cap' on the primary non-covalent ligand-binding site will be a general theme among members of the PDI family, as the current structural data on complexes with ligands are sparse. There is a recent structure of the ERp57–tapasin complex [18] and convincing models exist for ERp57 interactions within the MHC peptide-loading complex [18,33], and when bound to calnexin and a monoglucosylated protein folding intermediate [12,34]. However, the role of ERp57 in these complexes is rather different from that of PDI which we interpret as operating by using direct non-covalent binding interactions with the substrate (mainly involving **b′**) to destabilize the conformation of partially folded species while simultaneously catalysing disulfide interchange in the substrate through covalent interactions with the active sites in the **a** and **a′** domains.

The work in the present study shows that **b′** is a conformationally active domain that forms homodimers unless peptide ligands or the **x**-linker region are bound at its hydrophobic ligand-binding site. Ligand and **x** binding dissociate the dimer form and stabilize the tertiary structure. The binding of **x** is competitive with ligands and in fast exchange between two or more states. Controlled exposure of the hydrophobic binding site and the conformational properties of **b′** are likely to be key to the function of PDI. The **x**-linker region provides a mechanism for controlling access to the hydrophobic binding site and its displacement by substrate could initiate rearrangement of the domain architecture of PDI triggering changes in the protein folding activity by coupling the non-covalent substrate interactions at the **b′** domain with covalent substrate interactions with the redox-active sites on the **a** and **a′** domains. What is now required is to define better by both direct and indirect approaches, how ligand binding affects the relative orientations and dynamics of the various domains and sites within PDI.

AUTHOR CONTRIBUTION

Richard Williamson, Mark Howard, Robert Freedman and Lloyd Ruddock conceived the project, provided funding and guided the experimental work. Lloyd Ruddock generated and provided the plasmids encoding the various domain constructs. Ateesh Sidhu and Katrine Wallis expressed, purified and characterized the isotope-labelled proteins. Lee Byrne, Richard Williamson and Mark Howard recorded NMR spectra, and Lee Byrne, Katrine Wallis and Ateesh Sidhu assigned resonances. All of the authors contributed to data interpretation. Richard Williamson and Robert Freedman generated the first draft of the paper, Richard Williamson and Katrine Wallis generated the Figures, and all of the authors contributed to revision and approval of the final paper.

ACKNOWLEDGEMENTS

We thank Tom Frenkiel and Geoff Kelly at the Biomedical NMR Centre, National Institute of Medical Research, Mill Hill, London, U.K., for technical help and use of the Centre's NMR facilities, and the Mass Spectrometry Unit of the Department of Biological Sciences, Warwick University, for mass determination of recombinant proteins. We also thank Kevin Howland for peptide synthesis, Michelle Rowe for NMR support at Kent, and Annamari Ruddock for initial sample preparation.

FUNDING

This work was supported by the Biotechnology and Biological Sciences Research Council [grant number BB/D018072] and by a Biotechnology and Biological Sciences Research Council ear-marked studentship (to A. S.).

REFERENCES

1 Hatahet, F. and Ruddock, L. W. (2007) Substrate recognition by the protein disulfide isomerases. FEBS J. **274**, 5223–5234
2 Creighton, T. E. (1995) Disulphide-coupled protein folding pathways. Philos. Trans. R. Soc. London Ser. B **348**, 5–10
3 Freedman, R. B. (1995) The formation of protein disulphide bonds. Curr. Biol. **5**, 85–91
4 Land, A., Zonneveld, D. and Braakman, I. (2003) Folding of HIV-1 envelope glycoprotein involves extensive isomerisation of disulfide bonds and conformation-dependent leader peptide cleavage. FASEB J. **17**, 1058–1067

5 Freedman, R. B., Klappa, P. and Ruddock, L. W. (2002) Protein disulfide isomerases exploit synergy between catalytic and specific ligand-binding domains. EMBO Rep. **3**, 146–150

6 Ellgaard, L. and Ruddock, L. W. (2005) The human protein disulphide isomerase family: substrate interactions and functional properties. EMBO Rep. **6**, 28–32

7 Pirneskoski, A., Klappa, P., Lobell, M., Williamson, R. A., Byrne, L., Alanen, H. I., Salo, K. E. H., Kivirikko, K. I., Freedman, R. B. and Ruddock, L. W. (2004) Molecular characterization of the principal substrate binding site of the ubiquitous folding catalyst protein disulfide isomerase. J. Biol. Chem. **279**, 10374–10381

8 Klappa, P., Ruddock, L. W., Darby, N. J. and Freedman, R. . (1998) The b′ domain provides the principal peptide-binding site of protein disulfide isomerase but all domains contribute to binding of misfolded proteins. EMBO J. **17**, 927–935

9 Koivunen, P., Salo, K. E. H., Myllyharju, J. and Ruddock, L. W. (2005) Three binding sites in protein disulfide isomerase co-operate in collagen prolyl-4-hydroxylase tetramer assembly. J. Biol. Chem. **280**, 5227–5231

10 Darby, N. J., Penka, E. and Vincentelli, R. (1998) The multidomain structure of protein disulphide isomerase is essential for high catalytic efficiency. J. Mol. Biol. **276**, 2622–2636

11 Russell, S. L., Ruddock, L. W., Salo, K. E. H., Oliver, J. D., Roebuck, Q. P., Llewellyn, D. H., Roderick, H. L., Koivunen, P., Myllyharju, J. and High, S. (2004) The primary substrate binding site in the b′ domain of ERp57 is adapted for ER lectin association. J. Biol. Chem. **279**, 2501–2507

12 Kozlov, G., Maattanen, P., Schrag, J. D., Pollock, S., Cygler, M., Nagar, B., Thomas, D. Y. and Gehring, K. (2006) Crystal structure of the bb′ domains of the protein disulphide isomerase ERp57. Structure **14**, 1331–1339

13 Tian, G., Xiang, S., Noiva, R., Lennarz, W. J. and Schindelin, H. (2006) The crystal structure of yeast protein disulfide isomerase suggests cooperativity between its active sites. Cell **124**, 61–73

14 Tian, G., Kober, F.-X., Lewandrowski, U., Sickmann, A., Lennarz, W. J. and Schindelin, H. (2008) The catalytic activity of protein disulphide isomerase requires a conformationally flexible molecule. J. Biol. Chem. **283**, 33630–33640

15 Kemmink, J., Darby, N. J., Dijkstra, K., Nilges, M. and Creighton, T. E. (1996) Structure determination of the N-terminal thioredoxin-like domain of protein disulfide isomerase using multidimensional heteronuclear $^{13}C/^{15}N$ NMR spectroscopy. Biochemistry **35**, 7684–7691

16 Kemmink, J., Darby, N. J., Dijkstra, K., Nilges, M. and Creighton, T. E. (1997) The folding catalyst protein disulfide isomerase is constructed of active and inactive thioredoxin modules. Curr. Biol. **7**, 239–245

17 Wang, L., Wang, L., Vavassori, S., Li, S., Ke, H., Anelli, T., Degano, M., Ronzoni, R., Sitia, R., Sun, F. and Wang, C.-C. (2008) Crystal structure of human ERp44 shows a dynamic functional modulation of its carboxy-terminal tail. EMBO Rep. **9**, 642–647

18 Dong, G., Wearsch, P. A., Peaper, D. R., Cresswell, P. and Reinisch, K. M. (2009) Insights into MHC class I peptide loading from the structure of the tapasin–ERp57 thiol oxidoreductase heterodimer. Immunity **30**, 21–32

19 Kozlov, G., Määttänen, P., Schrag, J. D., Hura, G. L., Gabrielli, L., Cygler, M., Thomas, D. Y. and Gehring, K. (2009) Structure of the non-catalytic domains and global fold of the protein disulfide isomerase ERp72. Structure **17**, 651–659

20 Nguyen, V. D., Wallis, K., Howard, M. J., Haapalainen, A. M., Salo, K. E. H., Saaranen, M. J., Sidhu, A., Wierenga, R. K., Freedman, R. B., Ruddock, L. W. and Williamson, R. A. (2008) Alternative conformations of the x region of human protein disulphide-isomerase modulate exposure of the substrate-binding b′ domain. J. Mol. Biol. **383**, 1144–1155

21 Denisov, A. Y., Maattanen, P., Dabrowski, C., Kozlov, G., Thomas, D. Y. and Gehring, K. (2009) Solution structure of the bb′ domains of human protein disulfide isomerase. FEBS J. **276**, 1440–1449

22 Piotto, M., Saudek, V. and Sklenar, V. (1992) Gradient-tailored excitation for single-quantum NMR spectroscopy of aqueous solutions. J. Biomol. NMR **2**, 661–665

23 Alanen, H. I., Williamson, R. A., Howard, M. J., Hatahet, F. S., Salo, K. E. H., Kauppila, A., Kellokumpu, S. and Ruddock, L. W. (2006) ERp27, a new non-catalytic endoplasmic reticulum-located human protein disulfide isomerase family member, interacts with ERp57. J. Biol. Chem. **281**, 33727–33737

24 Grzesiek, S. and Bax, A. (1992) An efficient experiment for sequential backbone assignment of medium-sized isotopically enriched proteins J. Magn. Res. **99**, 201–207

25 Grzesiek, S. and Bax, A. (1992) Correlating backbone amide and side chain resonances in larger proteins by multiple relayed triple resonance NMR. J. Am. Chem. Soc. **114**, 6291–6293

26 Kemmink, J., Dijkstra, K., Mariani, M., Scheek, R. M., Penka, E., Nilges, M. and Darby, N. J. (1999) The structure in solution of the b domain of protein disulfide isomerase. J. Biomol. NMR **13**, 357–368

27 Delaglio, F., Grzesiek, S., Vuister, G. W., Zhu, G., Pfeifer, J. and Bax, A. (1995) NMRPipe: a multidimensional spectral processing system based on UNIX pipes. J. Biomol. NMR **6**, 277–293

28 Vranken, W. F., Boucher, W., Stevens, T. J., Fogh, R. H., Pajon, A., Llinas, M., Ulrich, E. L., Markley, J. L., Ionides, J. and Laue, E. D. (2005) The CCPN data model for NMR spectroscopy: development of a software pipeline. Proteins **59**, 687–696

29 Klappa, P., Freedman, R. B., Langenbuch, M., Lan, M. S., Robinson, G. K. and Ruddock, L. W. (2001) The pancreas-specific disulphide-isomerase PDIp interacts with a hydroxyl group in ligands. Biochem. J. **354**, 553–559

30 Tompa, P. and Csermely, P. (2004) The role of structural disorder in the function of RNA and protein chaperones. FASEB J. **18**, 1169–1175

31 Denisov, A. Y., Maattanen, P., Sprules, T., Thomas, D. Y. and Gehring, K. (2007) ^{1}H, ^{13}C and ^{15}N resonance assignments of the bb′ domains of human protein disulphide isomerase. Biomol. NMR Assign. **1**, 129–130

32 Jiang, J., Prasad, K., Lafer, E. M. and Sousa, R. (2005) Structural basis of interdomain communication in the Hsc70 chaperone. Mol. Cell **20**, 513–524

33 Elliott, T. (2009) More images that yet fresh images beget. Immunity **30**, 1–2

34 Ruddock, L. W. (2006) Gaining access to ERp57 function. Structure **14**, 1209–1210

35 Koradi, R., Billeter, M. and Wüthrich, K. (1996) MOLMOL: a program for display and analysis of macromolecular structures. J. Mol. Graphics **14**, 51–55

Received 9 April 2009/15 June 2009; accepted 15 July 2009
Published as BJ Immediate Publication 15 July 2009, doi:10.1042/BJ20090565